Galvanostatic Intermittent Titration Technique for Phase-Transformation Electrodes

Yujie Zhu and Chunsheng Wang*

Department of Chemical & Biomolecular Engineering, University of Maryland, College Park, Maryland 20742

Received: November 29, 2009

A novel galvanostatic intermittent titration technique (GITT) and a novel potentiostatic intermittent titration technique (PITT) for phase-transformation electrodes were developed by integrating mixed control phase-transformation theory with traditional GITT and PITT methods. The contribution of the strain accommodation energy to the thermodynamic driving force for phase transformation was assessed. These novel GITT and PITT methods can be used to determine the true ion diffusion coefficient and the interface mobility of phase-transformation electrodes in the two-phase region. To demonstrate the utility of this method, the lithium ion diffusion coefficient and the interface mobility of two $LiFePO_4$ samples with different particle sizes were obtained in the two-phase region. The lithium ion diffusion coefficient in the two-phase region as measured using phase-transformation GITT was on the order of 10^{-13} cm^2/s in the β phase ($Li_{1-y}FePO_4$) and 10^{-12} cm^2/s in the α phase (Li_xFeO_4), which is similar to the diffusion coefficients in the single β and single α phase regions determined using traditional GITT and PITT. This similarity with the diffusion-coefficient-validated phase-transformation GITT and PITT is expected since traditional GITT/PITT is reliable in the single-phase region. The interface mobility of the $LiFePO_4$ (about 10^{-15} m mol/J s) increases with decreasing particle size. The interface mobility of the $LiFePO_4/FePO_4$ during electrochemical discharge at room temperature is comparable to that of the martensite−austenite transformation in an Fe−C alloy with a semicoherence interface at 350 °C.

1. Introduction

Rechargeable lithium ion (Li ion) batteries are currently being used to power an increasingly diverse range of commercial products and have been recognized as a critical enabling technology for electric vehicles/hybrid electric vehicles (EV/HEV)[1] and renewable energy storage. Phase-transformation materials (such as $LiFePO_4$ and $Li_4Ti_5O_{12}$) are the most promising electrode materials for high-power Li ion batteries due to their fast reaction kinetics, safety, low cost, and long life. The high power density of the carbon-coated nano-$LiFePO_4$ electrode is attributed to (i) improved electronic conductivity through carbon coating[2] and supervalent cation doping,[3] (ii) a shortened ion/electron-transport path through the use of nano-sized materials,[4,5] and (iii) rapid phase transformation from a coherent or semicoherent interface between $Li_{1-y}FePO_4$ and Li_xFePO_4 due to a narrow miscibility gap in nanoscale $LiFePO_4$.[6−8] However, how the crystal structure, defects, and particle size affect the diffusion coefficient of lithium ions and the interface mobility of phase-transformation electrodes is still not fully understood[6,9−11] due to the lack of reliable electroanalytical techniques for measuring lithium ion transport in phase-transformation materials. All current electroanalytical methods, such as galvanostatic intermittent titration technique (GITT),[12] potentiostatic intermittent titration technique (PITT),[12] electrochemical impedance spectroscopy (EIS),[13] and cyclic voltammetry (CV),[14] can only be used to analyze ion transport in solid solution electrodes since they all rely on Fick's law of diffusion without considering the effect of interphase boundary movement on ion transport.

Using the traditional GITT method, the electrode system is subjected to a small constant current, and potential changes are measured as a function of time. Assuming one-dimensional diffusion in a solid solution electrode without consideration of ohmic potential drop, double-layer charging, charge-transfer kinetics, and phase transformation, the ion diffusion coefficient can be calculated using Fick's law through the following equation[12]

$$D_{\mathrm{GITT}} = \frac{4}{\pi}\left(\frac{IV_{\mathrm{M}}}{z_{\mathrm{A}}FS}\right)\left[\frac{(\mathrm{d}E(x)/\mathrm{d}x)}{(\mathrm{d}E(t)/\mathrm{d}\sqrt{t})}\right]^2 \qquad (t \ll L^2/D_{\mathrm{GITT}}) \tag{1}$$

where L (cm) is the characteristic length of electrode materials, F (C/mol) is the Faraday constant, z_A is the charge number of electroactive species (for a Li ion battery, $z_A = 1$), S (cm^2) is the contact area between the electrode and electrolyte, I (A) is the applied current, and V_M (cm^3/mol) is the molar volume of the electrode material. The value of $\mathrm{d}E(t)/\mathrm{d}t^{1/2}$ can be obtained from a plot of the voltage versus the square root of the time during constant current pulse, and $\mathrm{d}E(x)/\mathrm{d}x$ can be measured by plotting the equilibrium electrode voltage against the electroactive material composition after each current pulse.

Instead of a current pulse as in GITT, a small voltage step is applied to the system under the PITT method, and the resulting current is measured as a function of time. The diffusion coefficient of ions in solid solution electrodes can be estimated based on Fick's law using the following equation with the same assumptions as those made for GITT[12]

$$D_{\mathrm{PITT}} = -\frac{\mathrm{d}\ln I(t)}{\mathrm{d}t}\frac{4L^2}{\pi^2} \quad (t \gg L^2/D_{\mathrm{PITT}}) \tag{2}$$

* To whom correspondence should be addressed. Tel.: 301-405-0352. Fax: (301)314-9126. E-mail: cswang@umd.edu.

10.1021/jp9113333
Published on Web 01/22/2010

where L (cm) is the characteristic length of the electrode material and $I(t)$ (A) is the current measured during the constant voltage step.

Since both GITT and PITT are based on the same assumption of Fick's law, they are not reliable methods for measuring the ion diffusion coefficient in the two-phase region of phase-transformation materials. In the two-phase region, ions are transported through both movement of an interphase boundary and ionic diffusion. Using traditional electroanalytical techniques, only an apparent diffusion coefficient,[15−18] rather than the true diffusion coefficient, can be obtained in the two-phase region, which resulted in considerable controversy.[16,19−25] Moreover, the apparent Li ion diffusion coefficients of $LiFePO_4$ in the two-phase region measured using GITT,[19] PITT,[20] and EIS[20] were 2−3 orders of magnitude lower than those in the single-phase region. A reduced apparent diffusion coefficient in the two-phase region was also reported in $Li_4Ti_5O_{12}$ thin films measured using traditional PITT and EIS methods.[21] Since the Li ion diffusion coefficient in the single-phase region measured using traditional GITT and PITT is reliable, the significant reduction of the apparent diffusion coefficient in the two-phase region should be attributed to the phase transformation.

To address this problem, a moving boundary model[26,27] was proposed by taking into account the effect of phase transformation and assuming equilibrium conditions at the interphase boundary and no volume change, that is, no strain and stress. Since diffusion is considered to be the only factor controlling the boundary movement during phase transformation (corresponding to infinite interface mobility) in the moving boundary model, the Li ion diffusion coefficient obtained in the two-phase region is still significantly lower than that in the single-phase region.[16] However, the interface of phase-transformation electrodes propagates under nonequilibrium conditions as phase transformation is controlled by both diffusion and interface migration. The moving boundary model cannot reflect the real charge/discharge processes in phase-transformation electrodes. Since phase transformation is totally ignored in traditional GITT and PITT and is assumed to be controlled only by diffusion in the moving boundary model, the ion diffusion coefficient and interface mobility of phase-transformation electrodes in the two-phase region cannot be determined using traditional GITT/PITT or the moving boundary model.

In this paper, we clarify the coupling between ion diffusion and interface migration in the presence of strain accommodation energy (mechanical stress) due to misfit strain between the two phases. The chemical and mechanical contributions to the interface driving forces were determined, and the boundary conditions for the diffusion problem that is implied by interface kinetics were derived. Using this mixed control phase-transformation theory, we developed a novel GITT method, which for the first time allows precise measurement of the true ion diffusion coefficient and the interface mobility of phase-transformation electrodes in the two-phase region. Using the $LiFePO_4$ system as a specific example, we determined the Li ion diffusion coefficient and interface mobility in the two-phase region of two $LiFePO_4$ electrodes with average particle sizes of 500 nm and 1 μm, respectively, using phase-transformation GITT. Since the traditional GITT and PITT methods are considered to be reliable in the single-phase region, similarity between the values for the diffusion coefficient in the two-phase region ($Li_{1-y}FePO_4/Li_xFePO_4$) determined using phase-transformation GITT/PITT and the diffusion coefficient in the single-phase region ($Li_{1-y}FePO_4$ or Li_xFePO_4) determined using traditional GITT and PITT would serve as validation of the mixed control model and phase-transformation GITT. For the first time, the interface mobilities at different states of discharge (SoD) for two $LiFePO_4$ samples were also obtained.

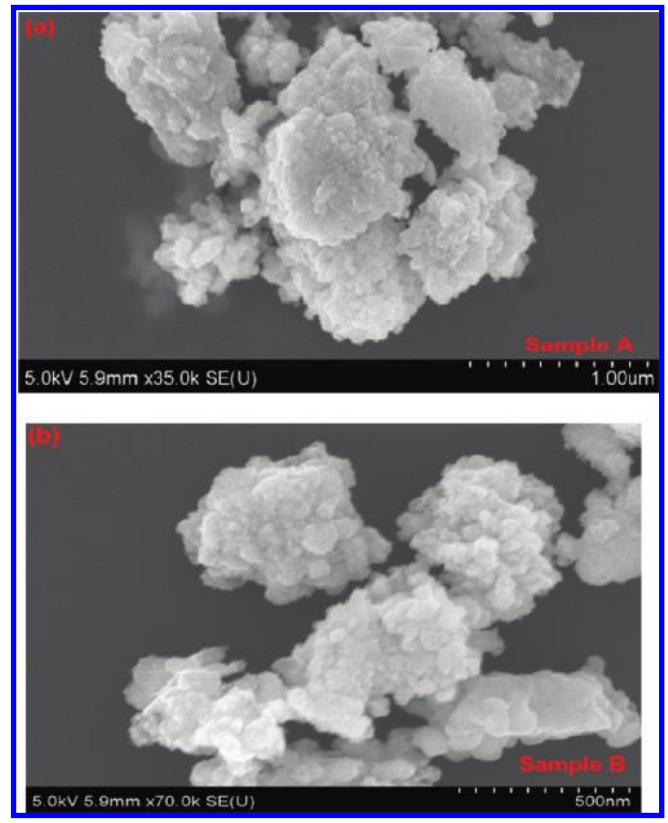

Figure 1. SEM images of two $LiFePO_4$ samples (a) sample A, ~1 μm primary particle aggregated from 100 nm secondary crystal particles, and (b) sample B, ~500 nm primary particle consisting of 40 nm secondary crystal particles.

2. Experimental Methods

Two carbon-coated $LiFePO_4$ samples with particle sizes of ~1 μm (sample A) and ~500 nm (sample B) were supplied by an industry in U.S.A. The 1 μm $LiFePO_4$ sample consisted of highly dense aggregates of secondary nanoscale crystal particles with an average size of 100 nm, as shown in Figure 1a. Similarly, the 500 nm $LiFePO_4$ particles were aggregates of secondary particles with an average size of about 40 nm, as shown in Figure 1b. Due to the high density, it is believed the electrolyte cannot penetrate into the $LiFePO_4$ particles through the nanocrystal grain boundary, and thus, the ion diffusion length should be half of the particle size rather than the crystal size (the size of the secondary particles). However, the crystal size will affect the strain accommodation energy and equilibrium potential in phase transformation.[6,7,28,29] The X-ray diffraction (XRD) patterns of the two $LiFePO_4$ samples, shown in Figure 2, demonstrate that the two commercial $LiFePO_4$ powders were in crystalline single phases.

A three-electrode pouch cell consisting of a $LiFePO_4$ cathode, a Li foil anode, a Li wire reference electrode, polypropylene (PP) microporous film separators, and 1.0 M $LiPF_6$ in EC−DEC−DMC−EMC (1:1:1:3 by volume) liquid electrolyte (Ferro Corporation) was used for electrochemical measurements. The $LiFePO_4$ electrodes were prepared using the slurry coating method. $LiFePO_4$ active materials were mixed with 10 wt % carbon black and 8 wt % polyvinylidene fluoride (PVDF) in 1-methyl-2-pyrrolidinone (NMP) solvent to form a viscous paste,

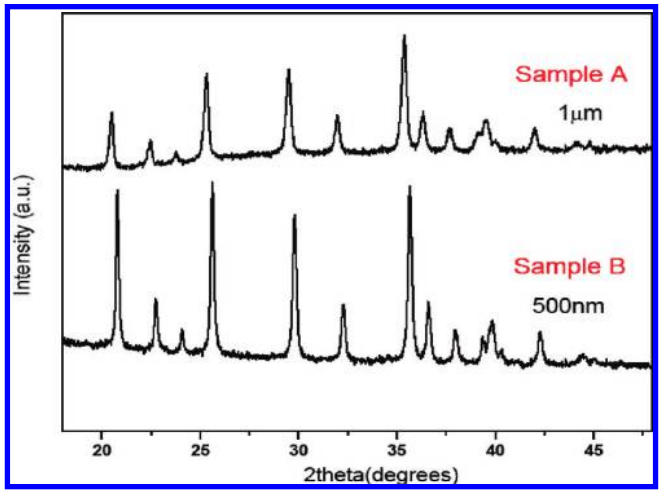

Figure 2. X-ray diffraction patterns of two $LiFePO_4$ samples.

which was then mixed for 45 min using a planetary ball milling machine. The paste obtained was then coated onto carbon-coated aluminum foil and dried in a vacuum oven at 120 °C overnight. After the foil cooled to room temperature, 2 cm × 2 cm electrodes with active material loading of 2 mg/cm^2 were cut out. GITT and PITT tests were performed on the three-electrode pouch cells after the $LiFePO_4$ electrodes were fully charged and discharged between 4.2 and 2.5 V for two cycles. GITT measurements consisting of a series of current pulses were applied to the three-electrode pouch cell at a low current of less than 0.05 C, each followed by a 16 h relaxation period. The relaxation time of 16 h was selected to allow full relaxation of the OCP (open-circuit potential), which requires more than 10 h[29] for 100 nm $LiFePO_4$, and to minimize the self-discharge of $LiFePO_4$ during the test. The potentials of 2.2 and 4.2 V were used as low and high cutoff voltages in GITT. In the PITT test, a series of potential steps of 20 mV each was applied to the $LiFePO_4$ electrodes in three-electrode pouch cells within a potential range of 4.1−3.5 V until the current was less than 0.01 C. To increase the accuracy in the two-phase region, a smaller potential step of 4 mV was used in the phase-transformation range (3.5−3.412 V).

3. GITT and PITT for Phase-Transformation Electrodes

3.1. General Discharge and Charge Process of Phase-Transformation Electrodes. Li ion insertion into phase-transformation electrodes is usually accompanied by initial dissolution of Li ions into the host materials to form a solid solution followed by phase transformation.[29] We denote the Li-poor phase as the α phase and the Li-rich phase as the β phase.

The phase-transformation process of electrodes during charge and discharge typically occurs as follows.

The potential−composition isotherm and Li ion concentration distribution during phase transformation is schematically represented in Figure 3. At the beginning of discharge (Li ion insertion), the Li ion enters the surface layer and continues to diffuse into the interior of the electrode particle. The Li ion concentration gradually increases, but the particle structure remains the same, forming a solid solution phase α. If there is no lattice misfit between the α phase and the newly formed β phase, once the theoretical solid solubility of the Li ion (C_α^e) in the α phase (at point b′ in Figure 3) is exceeded, the β phase should precipitate and grow in an α phase matrix. However, since there is a misfit accommodation energy induced by the molar volume difference between the α and the β phase, the β phase cannot deposit from the α phase until the Li ion concentration in the α phase reaches a value (corresponding to the point b in Figure 3a) which is higher than the theoretical solubility (point b′ in Figure 3a).[30,31] With the growth of the β phase during Li ion insertion, the misfit accommodation energy gradually accumulates, and the discharge equilibrium potential (E_{de}) continuously decreases (b−c line in Figure 3a). Once the α phase completely transforms into the β phase, subsequent Li ions will dissolve into the β phase and form a solid solution. Therefore, the discharge equilibrium potential decreases with Li ion concentration following the line a−b−c−d in Figure 3a. A reverse phase transformation occurs during charging (Li ion extraction) but at a higher potential (E_{ce}) than the theoretical (strain-free) potential E_{eq}. The charge equilibrium potential increases with Li ion extraction from $LiFePO_4$ following the line d−c−e−f−a in Figure 3a. A significant equilibrium potential hysteresis exists between discharge and charge, which is induced by the dissipation of energy to the surroundings due to elastic−plastic accommodation of strains resulting from the volume difference between the α and β phases.[32,33]

3.2. GITT and PITT Models Based on a Mixed Control Phase-Transformation Theory. We take the discharge process of phase-transformation electrodes as an example. The α to β phase transformation involves two processes. First, the β phase layer growth and interface migration occur simultaneously, which results in a gradual rearrangement of the lattice of parent phase α into the lattice of product phase β. Second, Li ion diffusion occurs from the particle surface into the interface through the β phase layer.

The driving force ΔG_d for phase transformation consists of three contributions, the chemical driving force ΔG_{chem}, the strain accommodation energy ΔG_{accom}, and the interface energy ΔG_{int}[34]

$$\Delta G_d = \Delta G_{chem} + \Delta G_{accom} + \Delta G_{int} \quad (3)$$

Compared to the chemical free energy and strain accommodation energy, the interface energy ΔG_{int} is small. For a planar interface, ΔG_{int} is equal to 0. Therefore, in this paper, we neglect the interface energy and only consider the chemical driving force and strain accommodation energy.

3.2.1. Chemical Driving Force ΔG_{chem} on an Interface. For a phase-transformation electrode, the following reaction takes place

$$Li_AH + (B - A)Li^+ + (B - A)e^- \underset{\text{delithiation}}{\overset{\text{lithiation}}{\rightleftharpoons}} Li_BH \quad (4)$$

where H stands for a host material, such as FePO4 in LiFePO4.

During the discharge process (lithiation), the chemical driving force ΔG_{chem} per mole of product material can be derived from the difference between the chemical potentials related to the corresponding host material H and the Li ion using the following equation

$$\Delta G_{chem} = B(\mu_{Li^+}^{\beta} - \mu_{Li^+}^{\alpha}) + (1 - B)(\mu_H^{\beta} - \mu_H^{\alpha}) \quad (5)$$

where B is the mole fraction of the Li ion (per mole of host material H) in the β phase. The chemical potentials in eq 5 disregard any mechanical force. Since the mobility of the Li ion is much higher than that of the host material and the interface

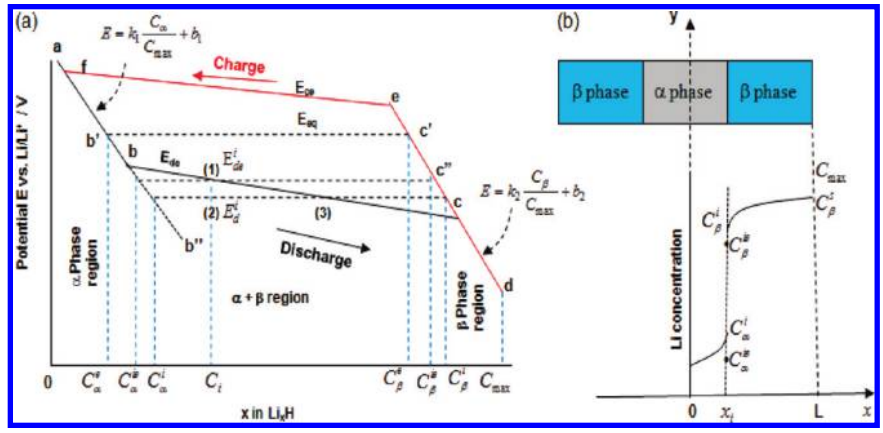

Figure 3. Schematic diagram of (a) a potential−composition isotherm and (b) the Li ion concentration distribution during discharge of phase-transformation materials.

is negligibly thin and sharp, the chemical potential of the Li ion across the sharp interface should be continuous

$$\mu^{\beta}_{Li^+} = \mu^{\alpha}_{Li^+} \tag{6}$$

The continuity of the carbon chemical potential across the interface between α-ferrite (or martensite) and γ-austenite has been well-recognized in Fe−C alloys.[34−37] The diffusion of interstitially dissolved carbon atoms across the interface between α-ferrite and γ-austenite in Fe−C alloys is similar to the diffusion of Li ions across the interface between the α and β phases in phase-transformation electrodes. A constant Li ion chemical potential across the α/β interface suggests that there exists a relationship between Li ion concentrations in the two phases at the interface,[35] which can be obtained by extrapolating the equilibrium potential lines of the α and β phases in the solid solution region (Figure 3a).[38] For example, when the electrode is dynamically discharged to state 2 in Figure 3a, the real interfacial potential (E^i_d) is lower than the corresponding equilibrium potential E^i_{de}, and the potential difference $E^i_d - E^i_{de}$ drives the phase transformation. Since the chemical potentials of the Li ion at the interface in the α and β phases are equal ($\mu^{\alpha}_{Li^+} = \mu^{\beta}_{Li^+}$), the dynamic interfacial concentration of Li ions in the α (C^i_α) and β phases (C^i_β) at the interface potential of E^i_d can be obtained by determining where the a−b and c−d lines intersect with the potential line at E^i_d in Figure 3a. The dynamic interfacial concentrations are higher than the corresponding equilibrium concentrations (C^{ie}_α for the α phase and C^{ie}_β for the β phase) at the strain-restricted equilibrium interfacial potential of E^i_{de} (state 1 in Figure 3a). However, the chemical potentials of the host material H at the interface are different in the α and β phases ($\mu^{\alpha}_H \neq \mu^{\beta}_H$). This chemical potential difference will drive the α phase lattice to transform to the β phase lattice and move the interface to state 3, where the chemical driving force $\mu^{\alpha}_H - \mu^{\beta}_H$ equilibrates to the accommodation energy. The chemical potentials of the Li ion and the host material H at the interface in the mixed control phase-transformation model ($\mu^{\alpha}_{Li^+} = \mu^{\beta}_{Li^+}$; $\mu^{\alpha}_H \neq \mu^{\beta}_H$) distinguish this model from the moving boundary model, which assumes that the interfacial chemical potentials of the Li ion and host material H in the α and β phases are always at equilibrium ($\mu^{\alpha}_{Li^+} = \mu^{\beta}_{Li^+}$; $\mu^{\alpha}_H = \mu^{\beta}_H$) during charge/discharge.

The chemical driving force of interface migration can be directly determined from the potential difference between the real interface potential E^i_d and the strain-free equilibrium potential E_{eq} using the Nernst equation. The Gibbs free-energy change based on one mole of host material H (reaction 4) at interface potential E^i_d (versus Li/Li$^+$) can be calculated using eq 7

$$\Delta G^i_d = -(B - A)FE^i_d \tag{7}$$

where F is the Faraday constant, B ($=C^i_\beta/C_{max}$) and A ($=C^i_\alpha/C_{max}$) are the mole fractions of the Li ion (per mole of host material H) in the β phase (Li_BH) and the α phase (Li_AH), respectively, and C_{max} (mol/cm^3) is the maximum Li ion concentration that can be incorporated into host material H. Similarly, the Gibbs free-energy change in reaction 4 based on one mole of host material H at the theoretical (strain-free) equilibrium potential of E_{eq} (versus Li/Li$^+$) can be calculated using eq 8. E_{eq} (versus Li/Li$^+$) can be estimated by averaging the charge and discharge equilibrium potentials (Figure 3a)

$$\Delta G_{eq} = -\left(\frac{C^e_\beta - C^e_\alpha}{C_{max}}\right)FE_{eq} \tag{8}$$

Therefore, the chemical driving force ΔG_{chem} at an interface potential of E^i_d can be expressed as

$$\Delta G_{chem} = \left(\frac{C^i_\beta - C^i_\alpha}{C_{max}}\right)FE^i_d - \left(\frac{C^e_\beta - C^e_\alpha}{C_{max}}\right)FE_{eq} \tag{9}$$

3.2.2. Mechanical Driving Force on an Interface. When the phase-transformation reaction involves any elastic−plastic strain, the α/β interface in the electrodes will not equilibrate at theoretical potential E_{eq} but at a lower potential of E^i_{de} to balance the accommodation energy induced by strain. Since the chemical driving force is equal to the accommodation energy at discharge equilibrium potential E_{de},[31] the accommodation energy can be calculated from the chemical free-energy difference

$$\Delta G_{accom} = \left(\frac{C^e_\beta - C^e_\alpha}{C_{max}}\right)FE_{eq} - \left(\frac{C^{ie}_\beta - C^{ie}_\alpha}{C_{max}}\right)FE^i_{de} = f(x_i) \tag{10}$$

The actual equilibrium potential of the electrode E^i_{de} during discharge can be determined using GITT. Since the accommodation energy accumulates during phase transformation,

ΔG_{accom} is a function of interface position x_i, which can be expressed as a function $f(x_i)$.

3.2.3. Total Driving Force ΔG_d for Phase Transformation. On the basis of the expressions of the chemical and mechanical driving force for phase transformation, the total driving force for phase transformation can be expressed as

$$\Delta G_d = \Delta G_{chem} + \Delta G_{accom} = \left(\frac{C_\beta^i}{C_{max}} - \frac{C_\alpha^i}{C_{max}}\right)FE_d^i - \left(\frac{C_\beta^{ie}}{C_{max}} - \frac{C_\alpha^{ie}}{C_{max}}\right)FE_{de}^i$$

or

$$\Delta G_d = \left(\frac{C_\beta^i}{C_{max}} - \frac{C_\alpha^i}{C_{max}}\right)FE_d^i - \left(\frac{C_\beta^e}{C_{max}} - \frac{C_\alpha^e}{C_{max}}\right)FE_{eq} + f(x_i) \quad (11)$$

where E_d^i is the actual interface potential, E_{de}^i is the strain-restricted equilibrium potential during discharge, which can be determined from GITT, and E_{eq} is the theoretical (strain-free) equilibrium potential.

3.2.4. Kinetics during Phase Transformation. The Li ion concentration distributions in the α and β phases when the interface is moving to the position x_i (composition C_i in Figure 3a) is schematically shown in Figure 3b. Under mixed control phase-transformation theory, the initial and boundary conditions for 1-D diffusion in GITT are listed as follows (assuming slab geometry).

In the α phase

$$\frac{\partial C_\alpha}{\partial t} = D_\alpha\left(\frac{\partial^2 C_\alpha}{\partial x^2}\right) \quad (12)$$

$$C_\alpha = C_\alpha^0 \qquad t = 0 \quad (13)$$

$$\frac{\partial C_\alpha}{\partial x} = 0 \qquad x = 0, \quad t \geq 0 \quad (14)$$

In the β phase

$$\frac{\partial C_\beta}{\partial t} = D_\beta\left(\frac{\partial^2 C_\beta}{\partial x^2}\right) \quad (15)$$

$$C_\beta = C_\beta^0 \qquad t = 0 \quad (16)$$

$$-D_\beta\left(\frac{\partial C_\beta}{\partial x}\right) = \frac{i\rho L}{z_A F} \qquad x = L, \quad t \geq 0 \quad (17)$$

As shown in Figure 3a, by extrapolating the equilibrium potential versus composition lines in the single α and β regions, the relationship between the discharge potential E and the Li ion concentration in the α phase (C_α) and β phase (C_β) can be approximately expressed as a linear relationship (Figure 3a)

$$E = k_1\frac{C_\alpha}{C_{max}} + b_1 \qquad \text{(for the α phase)} \quad (18)$$

$$E = k_2\frac{C_\beta}{C_{max}} + b_2 \qquad \text{(for the } \beta \text{ phase)} \quad (19)$$

where k_1 and k_2 are the slopes of the solubility versus equilibrium potential lines for single α and β phases and b_1 and b_2 are the intercepts.

For PITT, the boundary condition given by eq 17 becomes

$$x = L \qquad C_\beta = C_\beta^s \quad (20)$$

where C_β^scorresponds to the potential applied to the electrode during the PITT test, which can be determined using eq 19.

3.2.5. Interface Boundary Condition Determination. Performing a mass balance at the interface between the α and β phases gives

$$\frac{dx_i(t)}{dt} = \frac{D_\alpha\left(\frac{\partial C_\alpha}{\partial x}\right) - D_\beta\left(\frac{\partial C_\beta}{\partial x}\right)}{(C_\beta^i - C_\alpha^i)} \qquad x = x_i(t) \quad (21)$$

In eqs 11−21, C_α^0,C_β^0 and C_α^i,C_β^i are the initial and interfacial Li ion mole fractions in the α and β phases, D_α and D_β are the chemical diffusion coefficients of the Li ion in the α and β phases (cm^2/s), respectively, i is the current density (A/g) used in the test, ρ is the density of the phase-transformation material (g/cm^3), L is the characteristic length of the phase-transformation material (cm), $x_i(t)$ is the interface position, and z_A and F have the same meanings as in eq 1.

The interface velocity is linearly related to the chemical driving force ΔG_d by the interface mobility M[38]

$$\frac{dx_i(t)}{dt} = M\Delta G_d \quad (22)$$

The interface mobility M (m mol/(J s)) depends on the degree of interface coherence, the build up of stress, and deformations in the electrode materials.[38]

The interface boundary condition can be obtained by plugging eqs 11, 19, and 21 into eq 22

$$M\left[\left(\frac{C_\beta^i - C_\alpha^i}{C_{max}}\right)F\left(k_2\frac{C_\beta^i}{C_{max}} + b_2\right) - \left(\frac{C_\beta^e}{C_{max}} - \frac{C_\alpha^e}{C_{max}}\right) \times FE_{eq} + f(x_i)\right] = \frac{D_\alpha\left(\frac{\partial C_\alpha}{\partial x}\right) - D_\beta\left(\frac{\partial C_\beta}{\partial x}\right)}{(C_\beta^i - C_\alpha^i)} \quad (23)$$

Since the chemical potentials of the Li ion in the α and β phases should always be equal to each other at the interface, the Li ion concentration at the interface in the α phase is related to the Li ion concentration at the interface of the β phase, which can be obtained by combining eqs 18 and 19 at the interface

$$k_1\frac{C_\alpha^i}{C_{max}} + b_1 = k_2\frac{C_\beta^i}{C_{max}} + b_2 \quad (24)$$

It can be shown that when $b_1 = b_2$, eq 24 is reduced to the boundary condition used in ref 39.

Above all, eqs 12−17, 21, 23, and 24 consist of two partial differential equations (PDEs) and one ordinary differential equation (ODE) with corresponding initial and boundary conditions. By solving the above PDEs and ODE, we can determine the Li ion concentration profiles in both the α and β phases during phase transformation. All of the equations are converted to the dimensionless form and solved using the numerical method of lines (MOL) approach with the Maple software package. Details of the MOL approach can be found elsewhere[40,41] and will not be discussed here.

4. Application of Mixed Control Theory to $LiFePO_4$

Recent research has shown that the diffusion of Li ions is highly anisotropic in single-crystal $LiFePO_4$ particles, causing Li ions to be diffused mainly in a 1-D channel parallel to the *b* direction of the orthorhombic $LiFePO_4$ crystal structure.[42] Moreover, electron microscopy[43] and high-resolution electron energy loss spectroscopy (HREELS)[44] of chemically delithiated $LiFePO_4$ crystallites showed that the interface separating the α and β phases is parallel to the *bc* plane (perpendicular to the *a* axis), which suggested that Li ions diffuse through the interface between $FePO_4$ and $LiFePO_4$ with negligible transfer occurring in either the $FePO_4$ or $LiFePO_4$ phase (mechanism I in Figure 4a). The phase-transformation kinetics in single-crystal $LiFePO_4$ was investigated by Singh et al.[45] However, if multiple nano-$LiFePO_4$ crystals agglomerate to form a dense primary $LiFePO_4$ particle (SEM images in Figure 1), the process of Li ion insertion/extraction into these aggregated particles at the agglomerate scale can still be approximately described using mechanism II, where the interface between the α and β phases is parallel to the *ac* plane (perpendicular to the *b* axis, Figure 4b), although Li ion insertion into individual crystals follows mechanism I.[43,46] Mechanism II has been observed by Chen al etc.[47] in the phase decomposition of $LiFePO_4$, even though mechanism II requires slightly more energy than mechanism I.[48] In mechanism I, the phase boundary moves orthogonal to the direction of the surface flux, which indicates that the diffusion path does not change with the state of discharge (SoD) or state of charge (SoC). However, in mechanism II, the Li ion diffusion length increases with phase transformation (growth of the β phase). To verify whether the Li ion insertion into aggregated $LiFePO_4$ particles (Figure 1) can be approximately described by mechanism II, the variation of the diffusion overpotential with SoD and SoC of agglomerate $LiFePO_4$ was measured using GITT, as shown in Figure 5. It is clear that the discharge and charge overpotential of both agglomerates of $LiFePO_4$ increased with SoD and SoC, which means that the diffusion length was becoming longer, and the mixed control model (mechanism II) is valid for analyzing the phase-transformation process of agglomerate $LiFePO_4$. Moreover, the path dependence in the agglomerative $LiFePO_4$ observed by Srinivasan et al.[49] can also be reasonably explained using mechanism II.

To reduce the complexity of the problem, we assume that all of the diffusion channels of single-crystallite $LiFePO_4$ particles are arranged in the same direction in this study, which reduces the 3-D diffusion problem to a 1-D problem on the agglomerate scale (Figure 4b).

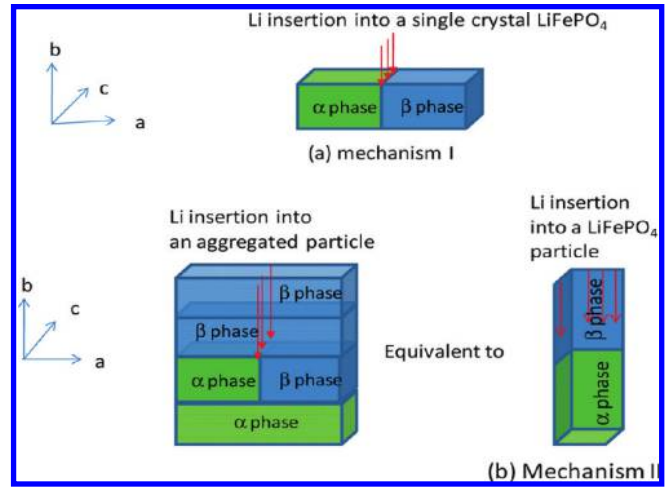

Figure 4. Schematic views of lithium intercalation mechanisms in a $LiFePO_4$ crystallite.

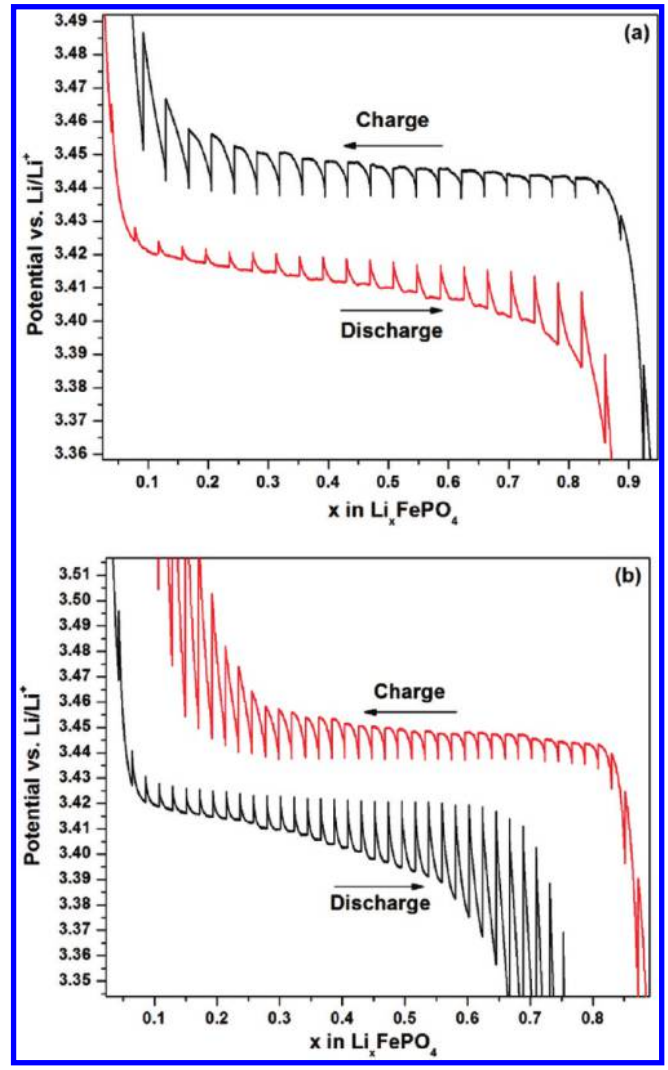

Figure 5. Charge/discharge GITT curves for (a) sample A and (b) sample B.

4.1. Parameter Determination. Most of the parameters for the diffusion coefficient and interface mobility calculations can be obtained from the curves of the charge/discharge equilibrium potential versus Li ion composition, which can be measured using GITT. As stated earlier, the strain-restricted discharge equilibrium potential E_{de} of $LiFePO_4$ can be determined using

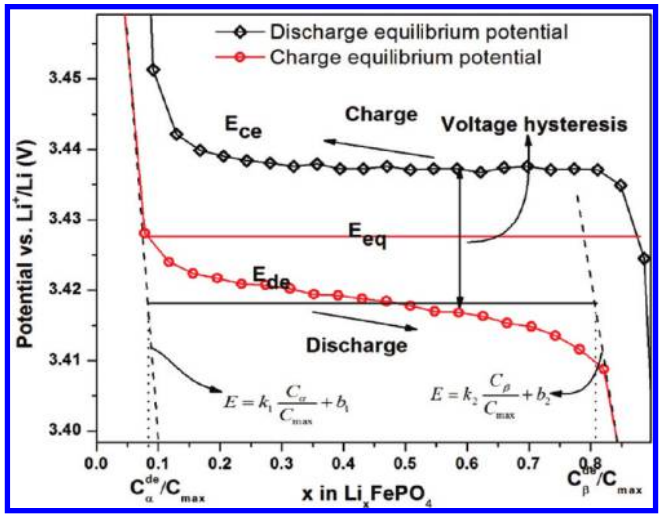

Figure 6. Equilibrium potential versus Li ion composition of sample A obtained using the GITT technique.

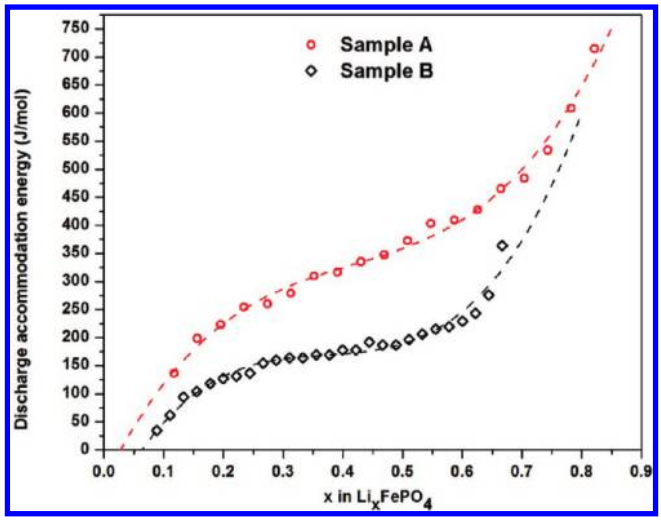

Figure 7. Discharge accommodation energies for samples A and B (experimental data: points; simulated data: dashed lines). The simulated discharge accommodation energies of samples A and B were calculated from $f_A(x_i) = 690.15 - 1429.50x_i + 2095.80x_i^2 - 1215.93x_i^3$ and $f_B(x_i) = 321.89 - 811.45x_i + 1500.93x_i^2 - 976.51x_i^3$, respectively.

GITT, and the theoretical (strain-free) equilibrium potential E_{eq} can be approximately estimated by averaging the discharge equilibrium potential E_{de} and charge equilibrium potential E_{ce}. The equilibrium concentrations C_α^e and C_β^e at E_{eq} and the concentrations C_α^{ie} and C_β^{ie} at different discharge equilibrium potentials E_{de} can be read from the GITT curves using the principle shown in Figure 3a. Figure 6 shows the charge/discharge equilibrium potential versus Li ion composition obtained using GITT for sample A.

The measured discharge accommodation energies obtained from eq 10 for samples A and B were plotted versus the Li ion concentration x in Li_xFePO_4 as points in Figure 7. To solve the above ODE and PDEs system, the measured accommodation energies at different Li ion insertion levels in Figure 7 were fitted using a third-order polynomial function $f(x_i)$, which are also shown as dash lines in Figure 7 for comparison. The calculated accommodation energies from $f(x_i)$ fit the measured values well, as shown in Figure 7. Sample B with small secondary particle size (<40 nm) had a lower accommodation energy than sample A with a large secondary particle size (>100 nm). The reduced accommodation energy of sample B is attributed to shrinking of the Li ion miscibility gap with decreasing particle size and to the high discharge equilibrium potential.[7,8] The parameters for concentrations and equilibrium potentials obtained from GITT of the two samples are listed in Table 1.

TABLE 1: Parameters Used for GITT and PITT Simulations

parameters	sample A	sample B
particle size (nm)	1000	500
second particle size (nm)	40	100
density of $FePO_4$ particle (ρ) (g/cm^3)	3.6	3.6
molar volume of $LiFePO_4$(cm^3/mol)	46	46
C_{max} (mol/cm^3)	0.02119	0.02119
C_α^e/C_{max}	0.041	0.042
C_β^e/C_{max}	0.768	0.864
current density for GITT (A/g)	0.0060	0.00350
strain-free equilibrium potential E_{eq} (V)	3.4276	3.4292
$\Delta G_{accom} = f(x_i)$ (J/mol)	$f(x_i) = 690.15 - 1429.50x_i + 2095.80x_i^2 - 1215.93x_i^3$	$f(x_i) = 321.89 - 811.45x_i + 1500.93x_i^2 - 976.51x_i^3$
k_1	−12.03	−5.99
b_1	3.94	3.68
k_2	−4.80	−3.42
b_2	7.57	6.04

4.2. Li Ion Diffusivity Obtained Using Phase-Transformation GITT. By solving the above model numerically at different initial conditions, we can obtain discharge curves at different SoDs. We can fit the experimental results to the simulated curves by changing parameters (D_α, D_β, and M) in the above model. Figure 8 shows typical discharge GITT curves of sample A at 10, 30, 60, and 90% SoD and simulated data using the mixed control phase-transformation GITT model at corresponding SoDs. As shown in Figure 8, the simulated discharge curves agreed well with the experimental data, with a deviation of less than 2 mV.

The D_α and D_β values obtained by fitting the GITT discharge curves in the two-phase region at different SoDs were plotted versus Li ion concentration x in Li_xFePO_4, as shown in Figure 9. For comparison, the apparent diffusion coefficients calculated using the traditional GITT method (eq 1) in both the single- and two-phase regions are also shown in Figure 9. As reported by other researchers,[19] the diffusion coefficients in the two-phase region obtained using traditional GITT are 3 orders of magnitude lower than those in the single-phase region. This result is unreasonable because the composition and structure of the α phase before and after β phase deposition is almost the same; therefore, the diffusion coefficient of the α phase should be similar to that during β phase formation. The reduced diffusion coefficient in the two-phase region calculated using traditional GITT is induced by a lower gradient of equilibrium potential ($dE(x)/dx$ in eq 1) in the two-phase region than that in two single-phase regions. Theoretically, the gradient of equilibrium potential of $LiFePO_4$ in the two-phase region should be 0, and the gradient of equilibrium potential in the two-phase region is induced by the strain accommodation energy. On the basis of traditional GITT, the diffusion coefficient of phase-transformation electrodes in the two-phase region will increase with accommodation energy, which is unreasonable. The diffusion coefficients in the α and β phases in the two-phase region determined using mixed control phase-transformation GITT are similar to the values in single-phase regions calculated from eq 1 using traditional GITT. Since the diffusion coefficient in

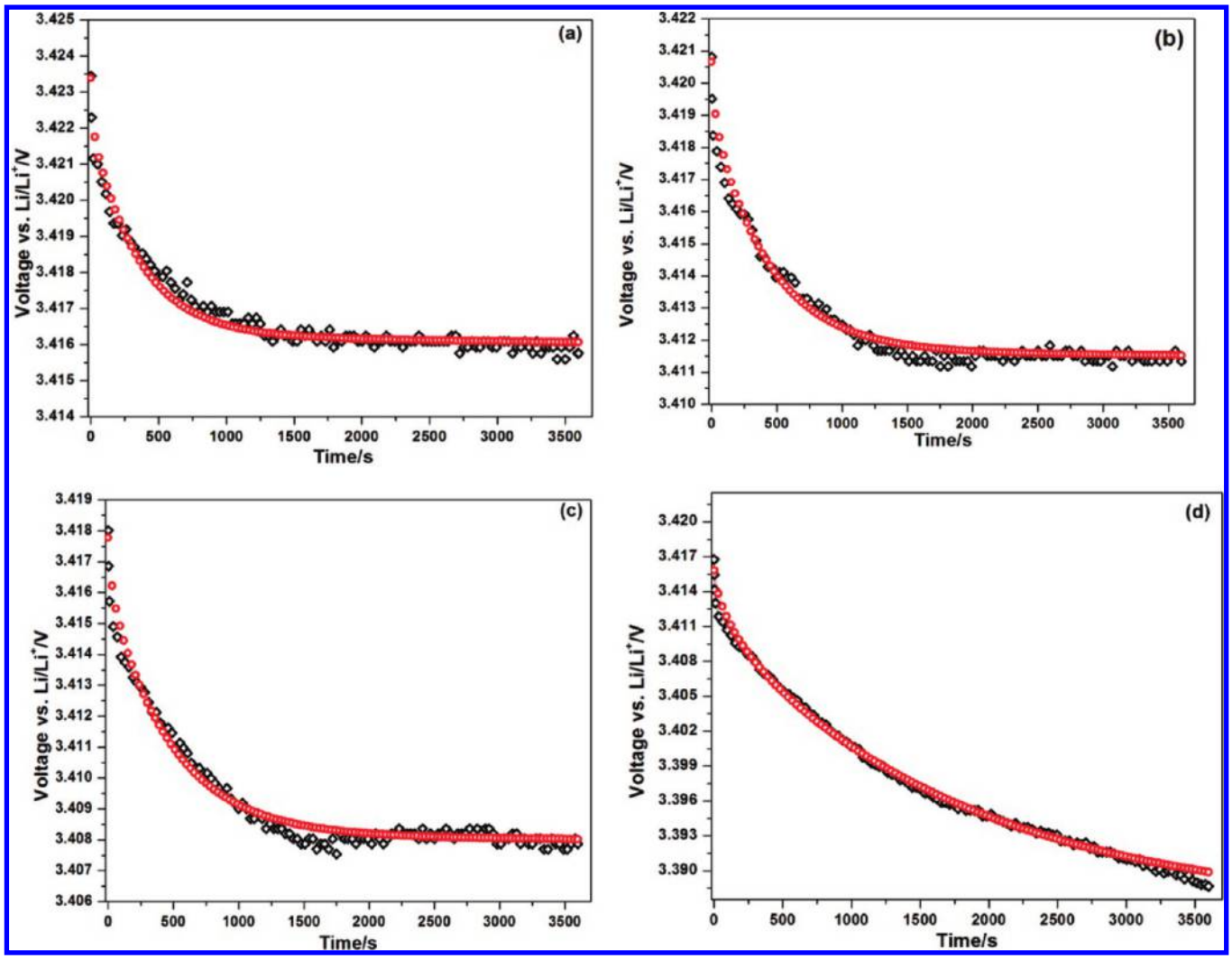

Figure 8. Experimental and simulated data of sample A at different SoDs (a) 10, (b) 30, (c) 60, and (d) 90%. (Black diamonds: experimental data; red circles: simulated data).

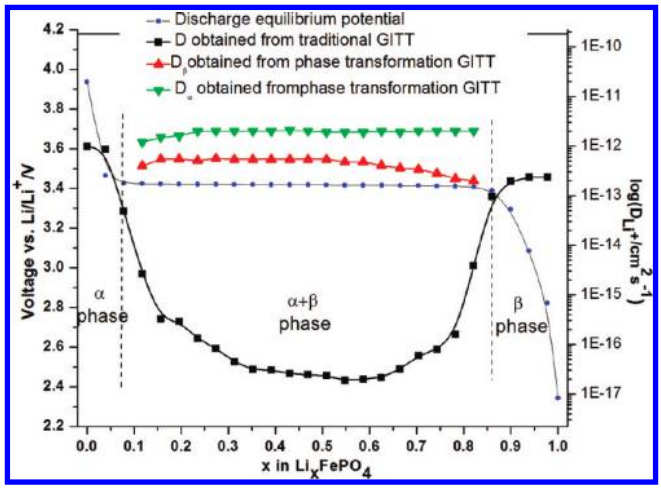

Figure 9. Li ion diffusion coefficients of sample A at different Li ion insertion levels using traditional discharge GITT and phase-transformation discharge GITT. The phase region is marked based on the discharge equilibrium−composition curve.

single-phase regions obtained using traditional GITT is reliable, the similarity between diffusion coefficients in the single-phase and two-phase region validated the new GITT method. The diffusion coefficient of the α phase is about 10^{-12} cm^2/s, which is 5−10 times higher than the diffusion coefficient in the β phase. The enhanced diffusion coefficient in the α phase agrees with theoretical predictions.[50] In Figure 9, the diffusion coefficient in the β phase decreases slightly with Li ion insertion, which may be attributed to gradually increased accommodation energy during the α to β phase transformation (Figure 7). Using traditional GITT (eq 1), we can only obtain one apparent diffusivity of α + β composite in the two-phase region without any information about Li ion diffusivity in either the α or β phase. However, by using the mixed control model, we obtained Li diffusivity in both the α and β phases in the two-phase region.

Figure 10 shows the experimental GITT data and well-fitted values for sample B at different SoDs. The obtained diffusion coefficients from fitting the experimental data to the model are shown in Figure 11. The diffusion coefficient measured using traditional GITT (eq 1) is also shown in Figure 11 for comparison. The diffusion coefficient in sample B is similar to the value in sample A. Therefore, the diffusion coefficient is not affected by the size of the secondary particle. As for sample A, the diffusion coefficients of sample B in the α and β phases in the two-phase region determined using mixed control phase-transformation GITT are similar to the values in single-phase regions calculated from eq 1 using traditional GITT. The diffusion coefficients of the two $LiFePO_4$ samples obtained using traditional GITT are in the same range as results from other

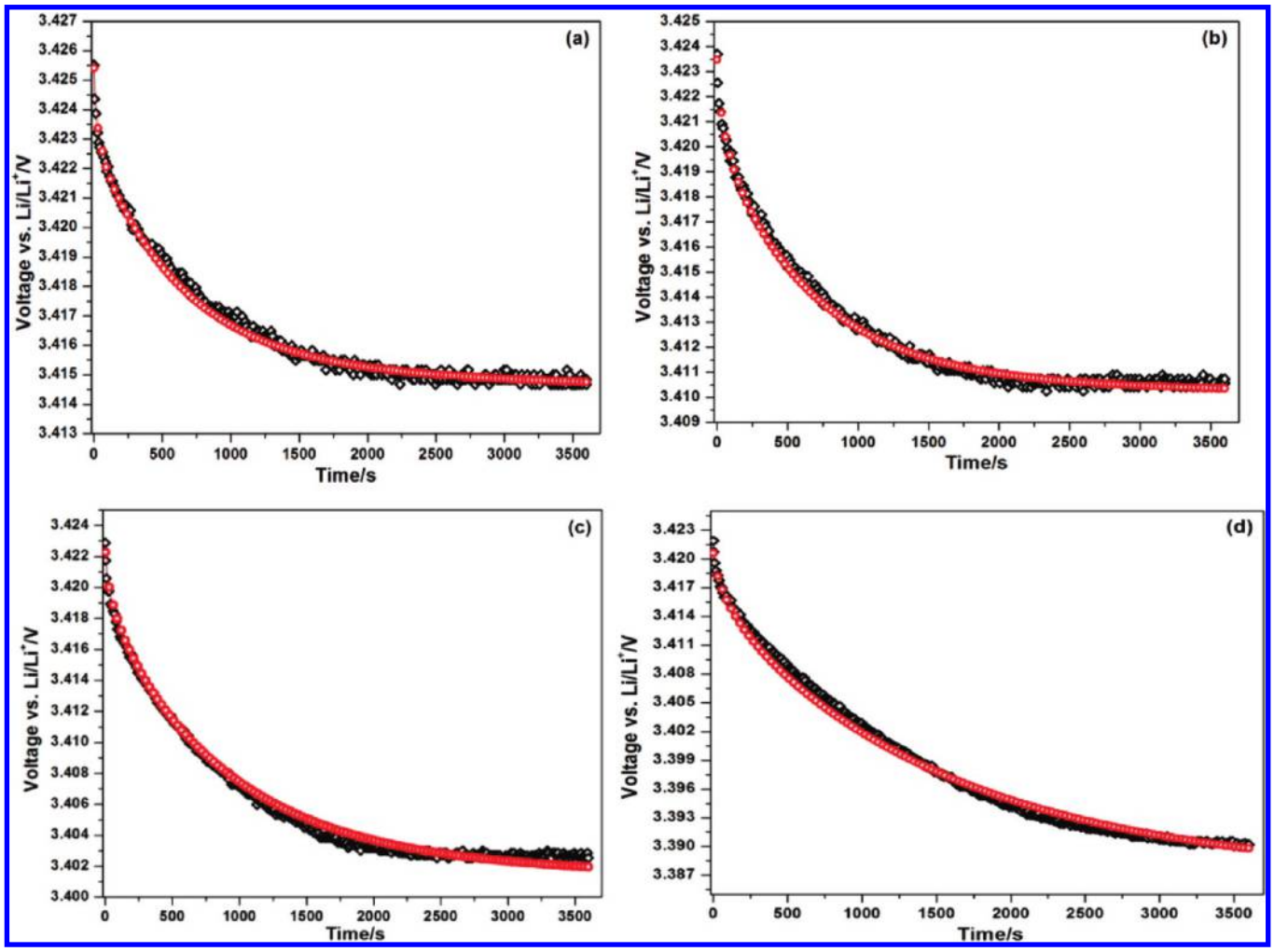

Figure 10. Experimental and simulated data of sample B at different SODs (a) 10, (b) 30, (c) 60, and (d) 90%. (Black diamonds: experimental data; red circles: simulated data).

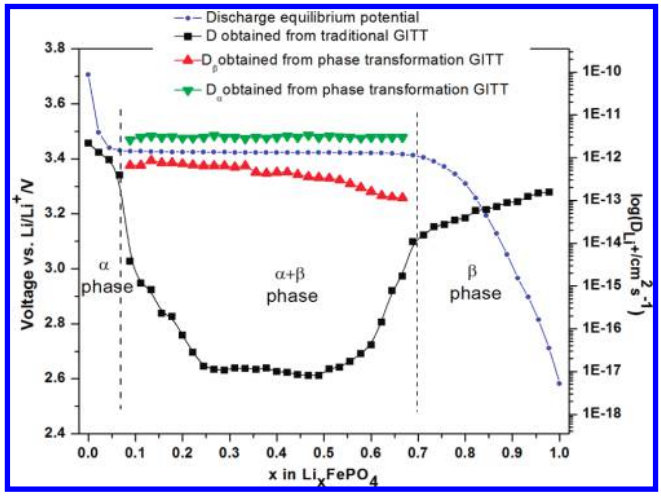

Figure 11. Li ion diffusion coefficients of sample B at different Li ion insertion levels using traditional discharge GITT and phase-transformation discharge GITT. The phase region is marked based on the discharge equilibrium−composition curve.

researchers (Table 2), indicating that the parameters obtained through GITT are reliable.

4.3. Li Ion Diffusivity Cross-checked by Mixed Control PITT. To further validate the phase-transformation GITT, the diffusion coefficient of the two $LiFePO_4$ samples was also cross-checked using the traditional PITT method (eq 2) and phase-transformation PITT. In the PITT measurement, potential steps of 20 mV in the single-phase region (3.00−3.41 V) and 4 mV in the two-phase region (3.43−3.41 V) were used. Since the potential range in the two-phase region is very narrow (less than 20 mV), only a few data points were obtained in the two-phase region. Two typical simulated current density versus time curves for sample B using phase-transformation PITT were compared with measured current density at different voltages in the two-phase region (Figure 12). The parameters in GITT fitting (Table 1) were used for fitting D_α, D_β, and M in PITT. The D_α and D_β obtained from phase-transformation PITT are plotted versus the voltage in Figure 13. For comparison, the diffusion coefficient of sample B in both single- and two-phase regions obtained using traditional PITT is also shown in Figure 13. Similar to traditional GITT, the diffusion coefficient obtained using traditional PITT in the two-phase region was also lower than

TABLE 2: Li Ion Diffusion Coefficient of $LiFePO_4$ Obtained Using Different Electroanalytical Techniques

technology	D_{Li}^+ in one phase region/cm^2s^{-1}	D_{Li}^+ in two phase region/cm^2s^{-1}	ref
GITT, EIS	$10^{-15}-10^{-14}$	$10^{-17}-10^{-16}$	19
PITT	$10^{-13}-10^{-12}$	$10^{-14}-10^{-13}$	20
EIS	10^{-13}	$10^{-15}-10^{-14}$	20
CITT	$10^{-15}-10^{-14}$	$10^{-16}-10^{-15}$	51
GITT/PITT	$10^{-14}-10^{-12}$	$10^{-18}-10^{-15}$	present work
new GITT/PITT		$10^{-14}-10^{-13}$	present work

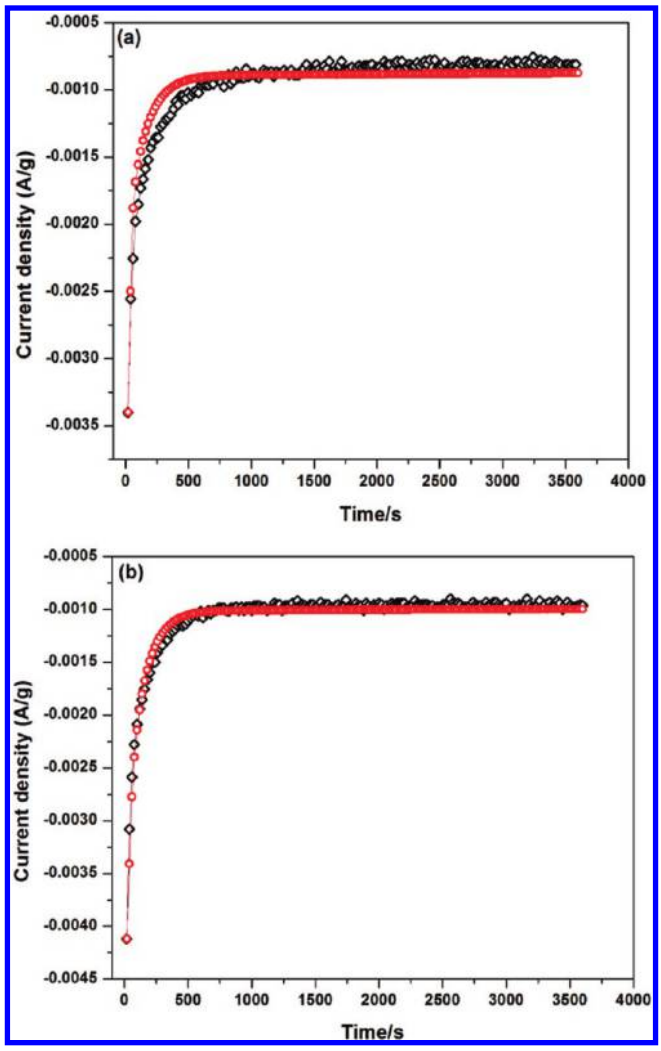

Figure 12. Comparing experimental data and simulated data in PITT for sample B; (a) voltage steps from 3.424 to 3.420 V; (b) voltage steps from 3.422 to 3.416 V.

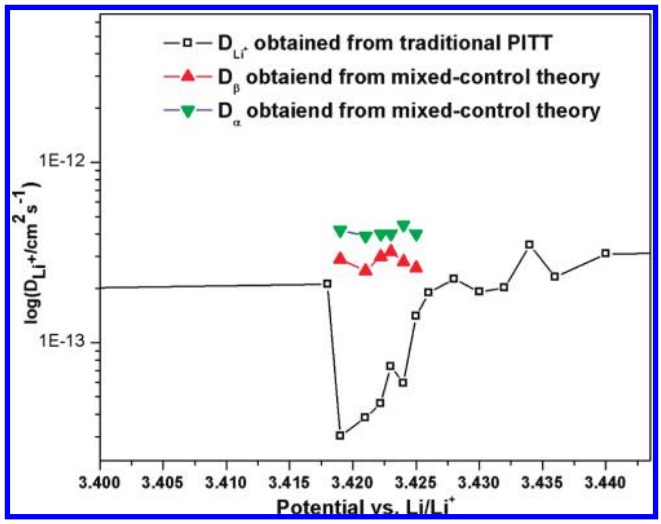

Figure 13. Li ion diffusivity calculated using traditional and phase-transformation PITT for sample B.

that in the single-phase region, while the diffusion coefficient (marked in Figure 12) obtained in the two-phase region using phase-transformation PITT is similar to the value in the single-phase obtained by traditional PITT. D_α and D_β in the two-phase region calculated using phase-transformation PITT are similar

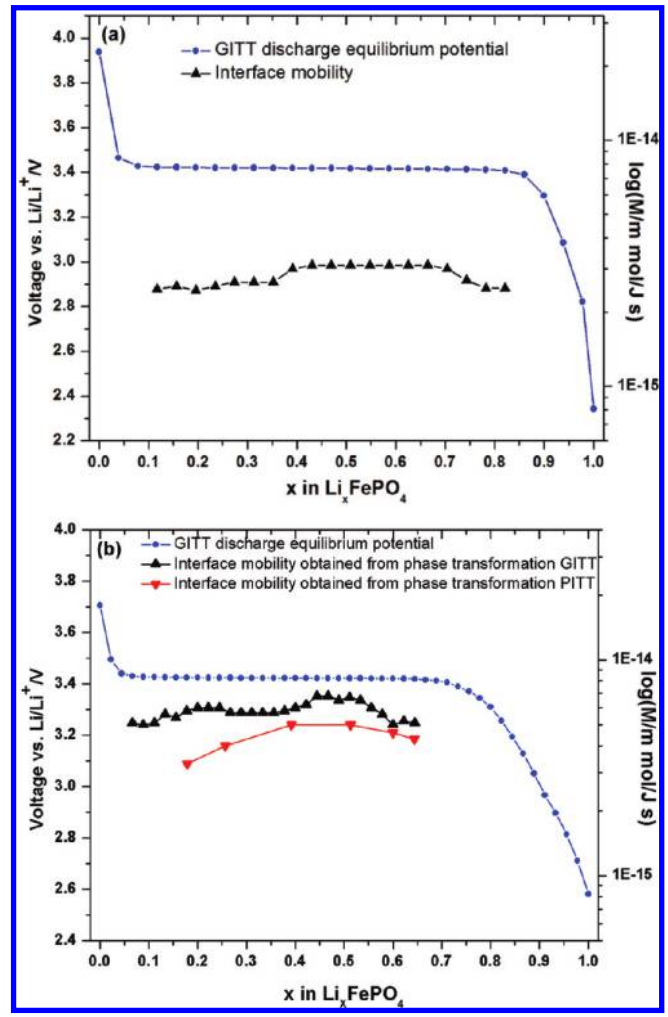

Figure 14. Interface mobilities of samples A and B obtained from phase-transformation GITT.

to the values obtained from phase-transformation GITT and in correspondence to the values in the single-phase region measured using traditional PITT, demonstrating the reliability of phase-transformation GITT and PITT.

4.4. Interface Mobility Obtained from Phase-Transformation GITT. In addition to the diffusion coefficient, the interface mobility M of the phase-transformation electrode can also be obtained using phase-transformation GITT and PITT. The interface mobilities of two $LiFePO_4$ samples at different SoDs are measured using phase-transformation GITT and PITT and are shown in Figure 14.

In Figure 14, the interface mobility M is about 10^{-15} m mol/(J s) for both samples. The average value of M (5.7×10^{-15} m mol/(J s)) for sample B with small secondary particles is 2 times higher than that of sample A (2.75×10^{-15} m mol/(J s)) with large secondary particles. Since the interface mobility depends on interface coherence, strain/stress, and deformations of the materials,[38] the high interface mobility of sample B may be attributed to the coherent interface and low accommodation energy for $LiFePO_4$ with small secondary particles. Sample B consisting of 40 nm secondary particle has a narrow miscibility gap (Figure 5), which decreases the lattice strain, as demonstrated by the low accommodation energy in Figure 6. The low lattice strain can potentially form a coherent interface between Li_xFePO_4 and $Li_{1-y}FePO_4$,[6] and the coherent interface causes high cooperative phase boundary movement upon electrochemical reaction with minimal formation of dislocations or cracks.[6]

The high interface mobility for small-size $LiFePO_4$ is in agreement with the reported results that the rate performance of $LiFePO_4$ increases with decreases in particle size.[6]

The interface mobility is usually temperature-dependent, which can be expressed as[52]

$$M = M_0 \exp\left(-\frac{Q_M}{RT}\right) \quad (25)$$

where M_0 is the pre-exponential factor which depends on the temperature and the average atomic spacing in two phases[52] and Q_M is the activation energy for interface movement, which is determined by the coherent/incoherent character of the interface between the two phases. Santofimia et al.[35] calculated the interface mobility of the martensite−austenite phase transformation. Their results showed that, at the annealing temperature of 350 °C, if the interface is coherent, the interface mobility is 2.45×10^{-20} m^4/(J s) (corresponding to 3.5×10^{-15} m mol/(J s)). The interface mobilities of the two $LiFePO_4$ samples studied in this paper are on the order of 10^{-15} m mol/(J s) at room temperature, which are similar to the interface mobility of the martensite−austenite phase transformation with a coherent interface at 350 °C.

5. Conclusion

Phase-transformation GITT and PITT methods were developed based on a mixed-control phase-transformation theory. Phase-transformation GITT and PITT can determine the accommodation energy, true diffusion coefficient, and interface mobility of phase-transformation electrodes during charge and discharge. These techniques can be applied to any ion insertion phase-transformation material, such as $LiFePO_4$, $Li_4Ti_5O_{12}$, and graphite for Li ion batteries and metal hydride materials for Ni/MH batteries. Applying phase-transformation GITT and PITT on two agglomerated $LiFePO_4$ electrodes with different secondary particle sizes, the effect of the crystal size of $LiFePO_4$ on the accommodation energy, diffusion coefficient, and interface mobility was investigated during discharge. The diffusion coefficient (10^{-11}−10^{-12} cm^2/s) in the α phase is 5−10 times higher than that in the β phase in the two-phase region, and the diffusion coefficient in the β phase slightly decreases with increasing SoD due to the increase in accommodation energy. The diffusion coefficients in the α phase and the β phase in the two-phase region are similar to the values in single α and single β regions. This contradicts all reported results that the diffusion coefficient in the two-phase region is 2−3 orders of magnitude lower than that in the single-phase region measured by using traditional GITT.

The accommodation energy and interface mobility of $LiFePO_4$ are size-dependent. $LiFePO_4$ with a 40 nm crystal size has a lower accommodation energy and higher interface mobility when compared to those for $LiFePO_4$ with a 100 nm crystal size. The interface mobility (10^{-15} m mol/(J s)) of $LiFePO_4$ at room temperature is comparable to the value for the martensite−austenite transformation in an Fe−C alloy with a semicoherent interface at 350 °C.

Acknowledgment. The authors gratefully acknowledge the support of the National Science Foundation under Contract No. CBET0933228 (Dr. Maria Burka, Program Director) and of the Army Research Office under Contract No. W911NF0810441 (Dr. Robert Mantz, Program Manager).

List of Symbols

A/B	mole fraction of the Li ion (per mole of host material H) at the interface in the α/β phase, %
b_1/b_2	intercept of the equilibrium potential versus solubility line for the single α/β phase, V
C_i	Li ion insertion concentration, mol/cm^3
C_{max}	maximum Li ion concentration that can be incorporated into the lattices of host material H, mol/cm^3
C_α/C_β,	Li ion concentration in the α/β phase during discharge, mol/cm^3
C_α^i/C_β^i	actual interfacial Li ion concentration in the α/β phase corresponding to potential E_d^i, mol/cm^3
$C_\alpha^{ie}/C_\beta^{ie}$	equilibrium interfacial Li ion concentration in the α/β phase corresponding to potential E_{de}^i, mol/cm^3
C_β^s	Li ion concentration at the electrode particle surface during PITT, mol/cm^3
C_α^e/C_β^e	theoretical Li ion solubility in the α/β phase corresponding to theoretical potential E_{eq}, mol/cm^3
D_{GITT}	Li ion diffusivity calculated using the traditional GITT method, cm^2/s
D_{PITT}	Li ion diffusivity calculated using the traditional PITT method, cm^2/s
D_α/D_β	Li ion diffusivity in the α/β phase, cm^2/s
E_d^i	actual potential of the α/β interface at any time during discharge, V
E_{de}^i	equilibrium potential of the α/β interface at any time during discharge, V
E_{de}/E_{ce}	discharge/charge equilibrium potential measured in GITT, V
E_{eq}	theoretical potential (strain-free potential) of the voltage plateau in GITT, V
$E(t)$	voltage measured as a function of time during the GITT test, V
$E(x)$	equilibrium potential measured as a function of the mole fraction of the Li ion during the GITT test, V
F	Faraday's constant, equal to 96500 C/mol
$f(x_i)$	expression of the accommodation energy as function of the interface position
H	host material of the electrode, such as $FePO_4$ in $LiFePO_4$
I	applied current in the traditional GITT method, A
i	current density used during discharge of GITT, A/g
$I(t)$	current measured as a function of time during the PITT test, A
k_1/k_2	slopes of the equilibrium potential versus the solubility line for the single α/β phase, V
L	characteristic length of the electrode material, cm
M	interface mobility of the α/β interface, m mol/(J s)
M_0	pre-exponential factor of the interface mobility equation, m mol/(J s)
Q_M	activation energy for interface movement, J/mol
R	universal gas constant, 8.314 J/(mol k)
S	contact area between the electrode and electrolyte, cm^2
t	time, s
T	temperature, K
V_M	molar volume of the electrode material, cm^3/mol
X	mole fraction of the Li ion in the electrode material, %
x_i	position of the interface boundary, cm
x	axial position in the particle, cm
z_A	charge number of the electroactive material; for Li ion batteries, $z_A = 1$
ΔG_d	total driving force during phase transformation, J/mol

ΔG_{chem} chemical driving force during phase transformation, J/mol

ΔG_{accom} strain-accommodation energy change during phase transformation, J/mol

ΔG_{int} interface energy change during phase transformation, J/mol

$\mu^{\alpha}_{Li^+}/\mu^{\beta}_{Li^+}$ chemical potential of the Li ion in the a/β phase at the interface, J/mol

$\mu^{\alpha}_{H}/\mu^{\beta}_{H}$ chemical potential of host material H in the α/β phase at the interface, J/mol

ρ density of electrode host material H, g/cm^3

References and Notes

(1) Chalk, S. G.; Miller, J. F. *J. Power Sources* **2006**, *159*, 73.

(2) Doeff, M. M.; X Hu, M. M.; McLarnon, F.; Kostecki, F. *Electrochem. Solid-State Lett.* **2003**, *6*, A207.

(3) Chung, S.-Y.; Blocking, J. T.; Chiang, Y.-M. *Nat. Mater.* **2002**, *1*, 123.

(4) Sides, C. R.; Croce, F.; Young, V. Y.; Martion, C. R.; Scrosati, B. *Electrochem. Solid-State Lett.* **2005**, *8*, A484.

(5) Kim, D.-H.; Kim, J. *Electrochem. Solid-State Lett.* **2006**, *9*, A439.

(6) Meetong, N.; Huang, H.; Speakman, S.; Carter, W. C.; Chiang, Y. M. *Adv. Funct. Mater.* **2007**, *17*, 1115–1123.

(7) Meetong, N.; Huang, H.; Carter, W. C.; Chiang, Y. M. *Electrochem. Solid-State Lett.* **2007**, *10*, A134–A138.

(8) Burch, D.; Bazant, M. Z. *Nano Lett.* **2009**, *9*, 3795.

(9) Subramanya Herle, P.; Ellis, B.; Coombs, N.; Nazar, L. F. *Nat. Mater.* **2004**, *3*, 147.

(10) Wang, C.; Hong, J. *Electrochem. Solid-State Lett.* **2007**, *10*, A65.

(11) Funabiki, A.; Inaba, M.; Abe, T.; Ogumi, Z. *J. Electrochem. Soc.* **1999**, *146*, 2443.

(12) Wen, C. J.; Boukamp, B. A.; Huggins, R. A. *J. Electrochem. Soc.* **1979**, *126*, 2258.

(13) Ho, C.; Raistrick, I. D.; Huggins, R. A. *J. Electrochem. Soc.* **1980**, *127*, 345.

(14) Bard, J.; Faulkner, L. R. *Electrochemical Methods*; Wiley Press: New York, 1980.

(15) Shin, H. C.; Pyun, S. I. *Electrochim. Acta* **1999**, *45*, 489.

(16) Levi, M. D.; Markevich, E.; Aurbach, D. *J. Phys. Chem. B* **2005**, *109*, 7420.

(17) Shin, H. C.; Pyun, S. I. *Electrochim. Acta* **1999**, *44*, 2235.

(18) Levi, M. D.; Markevich, E.; Aurbach, D. *Electrochim. Acta* **2005**, *5*, 1–98.

(19) Prosini, P. P.; Lisi, M.; Zane, D.; Pasquali, M. *Solid State Ionics* **2002**, *148*, 45–51.

(20) Xie, J.; Imanishi, N.; Zhang, T.; Hirano, A.; Takeda, Y.; Yamamoto, O. *Electrochim. Acta* **2009**, *54*, 4631–4637.

(21) Rho, Y. H.; Kanamura, K. *J. Solid State Chem.* **2004**, *177*, 2094–2100.

(22) Markevich, E.; Levi, M. D.; Aurbach, D. *J. Electranal. Chem.* **2005**, *580*, 231.

(23) Levi, M. D.; Aurbach, D. *Solid State Electrochem.* **2007**, *11*, 1031.

(24) Gaberscek, M.; Dominko, R.; Jamnik, J. *J. Power Sources* **2007**, *174*, 944.

(25) Yu, D. Y. W.; Fietzek, C.; Weydanz, W.; Donoue, K.; Inoue, T.; Kurokawa, H.; Fujitani, S. *J. Electrochem. Soc.* **2007**, *154*, A253.

(26) Funabiki, A.; Inaba, M.; Abe, T.; Ogumi, Z. *J. Electrochem. Soc.* **1999**, *146*, 2443.

(27) Levi, M. D.; Aurbach, D. *Electrochim. Acta* **1999**, *45*, 167.

(28) Kobayashi, G.; Nashimura, S. I.; Park, M. S.; Kanno, R.; Yashima, M.; Ida, T.; Yamada, A. *Adv. Funct. Mater.* **2009**, *19*, 395.

(29) Meethong, N.; Kao, Y. H.; Tang, M.; Huang, H. Y.; Carter, W. C.; Chiang, Y. M. *Chem. Mater.* **2008**, *20*, 6189.

(30) Krenn, C. R. *Model. Simul. Mater. Sci. Eng.* **2004**, *12*, S415.

(31) Hirai, K.; Ichitsubo, T.; Uda, T.; Miyzaki, A.; Yagi, S.; Matsubara, E. *Acta Mater.* **2008**, *56*, 1539.

(32) Allen, J. L.; Jow, T. R.; Wolfenstine, J. *Chem. Mater.* **2007**, *19*, 2108.

(33) Wang, X. P.; Corbel, G.; Kodjikian, S.; Fang, Q. F.; Lacorre, P. *J. Solid State Chem.* **2006**, *179*, 3338.

(34) Gamsjager, E.; Antretter, T.; Schmaranzer, C.; Preis, W.; Chimani, C. M.; Simha, N. K.; Svoboda, J.; Fischer, F. D. *Comput. Mater. Sci.* **2002**, *25*, 92.

(35) Santofimia, M. J.; Zhao, L.; Sietsma, J. *Scr. Mater.* **2008**, *59*, 159.

(36) Santofimia, M. J.; Speer, J. G.; Clarke, A. J.; Zhao, L.; Sietsma, J. *Acta Mater.* **2009**, *7*, 4548.

(37) Speer, J. G.; Hackenberg, R. E.; Decooman, B. C.; Matlok, D. K. *Philos. Mag. Lett.* **2007**, *87*, 379.

(38) Porter, D. A.; Easterling, K. E. *Phase Transformations in Metals and Alloys*, 2nd ed.; Chapman & Hall: London, 1992.

(39) Wang, C.; Kasavajjula, U.; Arce, P. E. *J. Phys. Chem. C* **2007**, *111*, 16656.

(40) Nowak, U. *Appl. Numer. Math.* **1996**, *20*, 129.

(41) Zhang, W. *Appl. Numer. Math.* **1996**, *20*, 235.

(42) Morgan, D.; Ven, A. V. D.; Ceder, G. *Electrochem. Solid-State Lett.* **2004**, *7*, A30.

(43) Chen, G. Y.; Song, X. Y.; Richardson, T. J. *Electrochem. Solid-State Lett.* **2006**, *9*, A295.

(44) Laffont, L.; et al. *Chem. Mater.* **2006**, *18*, 5520.

(45) Singh, G. K.; Ceder, G.; Bazant, M. Z. *Electrochim. Acta* **2008**, *53*, 7599.

(46) Delmas, C.; Maccario, M.; Croguennec, L.; Le Cras, F.; Weill, F. *Nat. Mater.* **2008**, *7*, 665.

(47) Chen, G. Y.; Song, X. Y.; Richardson, T. J. *J. Electrochem. Soc.* **2007**, *154*, A627.

(48) Ven, A. V. D.; Garikipati, K.; Kim, S.; Wagemaker, M. *J. Electrochem. Soc.* **2009**, *156*, A949.

(49) Srinivasan, G. V.; Newman, J. *Electrochem. Solid-State Lett.* **2006**, *9*, A110.

(50) Morgan, D.; Van der Ven, A.; Ceder, G. *Electrochem. Solid-State Lett.* **2004**, *7*, A30.

(51) Tang, X.-C.; Li, L.-X.; Lai, Q.-L.; Song, X.-W.; Jiang, L.-H. *Electrochim. Acta* **2009**, *54*, 2329.

(52) Thiessen, R. G.; Richardson, I. M.; Sietsma, J. *J. Mater. Sci. Eng.* **2006**, *A427*, 223.

JP9113333